
LEARNING GENERAL REPRESENTATION OF 12-LEAD ELECTROCARDIOGRAM WITH A JOINT-EMBEDDING PREDICTIVE ARCHITECTURE

Sehun Kim

Department of Mathematical Science,
Seoul National University
shunhun33@snu.ac.kr

ABSTRACT

We propose a self-supervised learning method for 12-lead Electrocardiogram (ECG) analysis, named ECG Joint Embedding Predictive Architecture (ECG-JEPA). ECG-JEPA employs a masking strategy to learn semantic representations of ECG data. Unlike existing methods, ECG-JEPA predicts at the hidden representation level rather than reconstructing raw data. This approach offers several advantages in the ECG domain: (1) it avoids producing unnecessary details, such as noise, which is common in standard ECG; and (2) it addresses the limitations of naïve L2 loss between raw signals. Another key contribution is the introduction of a special masked attention tailored for 12-lead ECG data, Cross-Pattern Attention (CroPA). CroPA enables the model to effectively capture inter-patch relationships. Additionally, ECG-JEPA is highly scalable, allowing efficient training on large datasets. Our code is openly available https://github.com/sehunfromdaegu/ECG_JEPA.

1 Introduction

Electrocardiograms (ECG) provide a non-invasive method to measure the electrical activity of the heart over time, serving as a crucial tool for diagnosing various cardiac conditions. While numerous supervised learning models have been developed to detect heart diseases using ECG data [1, 2, 3], these models often face significant performance degradation when applied to data distributions different from those on which they were trained.

Self-supervised learning (SSL) has emerged as a powerful paradigm for learning general representations across various domains, including natural language processing [4, 5, 6], computer vision [7, 8, 9], and video analysis [10, 11]. Despite its promise, applying SSL to ECG data presents unique challenges. For instance, data augmentation, which is essential in many SSL architectures, is more complex for ECG than for computer vision (CV) data. Simple transformations like rotation, scaling, and flipping, effective in CV, can distort the physiological meaning of ECG signals. Additionally, ECG recordings often contain artifacts and noise, which cause autoencoder-based SSL models to struggle with reconstructing raw signals. These architectures may also miss visually subtle but diagnostically critical features, such as P-waves and T-waves, which are imperative for diagnosing certain cardiac conditions.

In this work, we propose a novel ECG Joint-Embedding Predictive Architecture (ECG-JEPA) tailored for 12-lead ECG data, effectively addressing the aforementioned challenges. ECG-JEPA utilizes a transformer architecture to capture the semantic meanings of ECG. By masking several patches of the ECG data, ECG-JEPA predicts the abstract representations of the missing patches, indicating a high-level understanding of the data. Additionally, we develop a novel masked-attention for multi-lead ECG data, coined Cross-Pattern Attention (CroPA). CroPA enables the transformer architecture to effectively capture the relationships between patches in multi-lead ECG.

In this work, we demonstrate that:

- ECG-JEPA significantly improves linear evaluation and fine-tuning on classification tasks compared to existing SSL methods without hand-crafted augmentations.

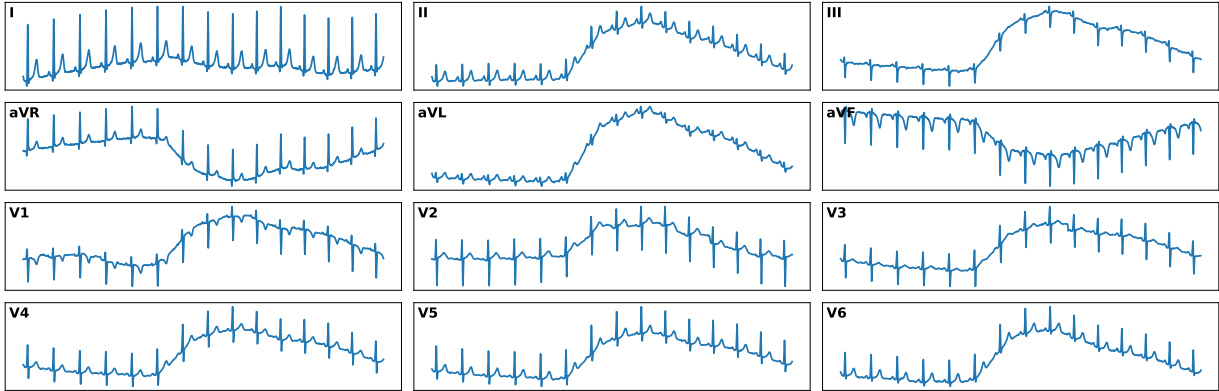


Figure 1: **12-lead ECG.** The standard 12-lead ECG captures electrical activity from different angles around the heart, providing comprehensive cardiac assessment. Artifacts and noise, such as powerline interference and baseline wander, are common in ECG recordings. The figure shows an example of a 12-lead ECG with baseline wander.

- CroPA enhances the model’s ability to capture inter-lead relationships, leading to better performance on downstream tasks.
- ECG-JEPA can also recover important ECG features, including heart rate and QRS duration, which are classical indicators used in ECG evaluation. This is the first work to demonstrate that learned representations can effectively recover various ECG features.
- ECG-JEPA is highly scalable, allowing efficient training on large datasets. For instance, ECG-JEPA is trained for only 100 epochs, yet outperforms other ECG SSL models on most downstream tasks, taking approximately 26 hours on a single RTX 3090 GPU.

2 Background

Self-Supervised Learning (SSL) facilitates learning abstract representations from input data without the need for labeled data, which is particularly beneficial in medical domains where labeled data is scarce and expensive. SSL leverages inherent data patterns to learn useful representations, allowing models to adapt to various downstream tasks with greater robustness to data imbalances [12].

2.1 Generative Architectures

Generative architectures involve reconstructing an input x from its degraded version x' using an encoder-decoder framework. The idea behind generative architectures is that the ability to reconstruct the clean data from a corrupted one indicates a good understanding of the data. The encoder maps the perturbed input x' into a latent representation, which the decoder then uses to generate the original input x [13].

2.2 Joint-Embedding Predictive Architectures

Joint-Embedding Predictive Architectures (JEPA) [14] process pairs x and their corrupted versions x' to obtain representations z and z' through encoders. Unlike generative architectures that predict in the input space, JEPA predicts in the hidden representation space by reconstructing z from z' . This approach effectively avoids the challenge of predicting unpredictable details, which is common in biological signals.

2.3 Electrocardiogram (ECG)

The electrocardiogram (ECG) is a non-invasive diagnostic method that records the heart’s electrical activity over time using electrodes placed on the skin. The standard 12-lead ECG captures electrical activity from multiple angles. These 12 leads are categorized into limb leads (I, II, III), augmented limb leads (aVR, aVL, aVF), and chest leads (V1-V6). Each lead provides unique information about the heart’s electrical activity, offering a comprehensive view that aids in diagnosing various cardiac conditions. Refer to Figure 1 for an illustration.

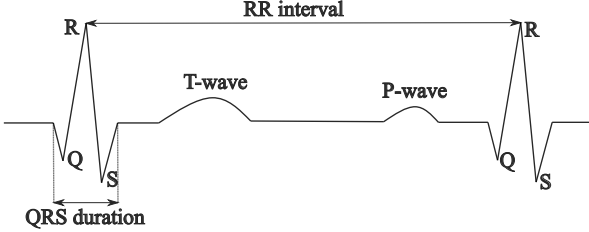


Figure 2: **Key ECG Features.**

In this work, we use only 8 leads (I, II, V1-V6) as the remaining 4 leads (III, aVR, aVL, aVF) can be derived from linear combinations of the 8 leads. This choice maintains the necessary diagnostic information while optimizing computational efficiency.

2.4 ECG Features

ECG features are specific characteristics of ECG signals that are critical for summarizing the overall signal. These features play an essential role in monitoring a patient’s health status and are instrumental in the application of statistical machine learning models for diagnosing heart diseases. Key ECG features include heart rate, QRS duration, PR interval, QT interval, and ST segment. These features are identified by measuring specific time intervals or amplitude levels in the ECG waveform. For instance, heart rate is calculated using the formula $1000 \times (60/\text{RR interval})$, where the RR interval is measured in milliseconds (ms). Refer to Figure 2 for a visual representation of these features.

3 Methodology

ECG-JEPA is trained by predicting masked representations of ECG data within the hidden representation space, using only a partial view of the input. The proposed architecture utilizes a student-teacher network framework, as illustrated in Figure 3. We subdivide the multi-channel ECG into non-overlapping patches and sample a subset of these patches for masking. However, reconstructing the raw signals of masked patches can be particularly challenging in the ECG domain due to the prevalence of noise in biological signals. Instead, our model predicts the masked patches in the hidden representation space, where this challenge can be effectively addressed. We validate the quality of the learned representations through various downstream tasks, including linear probing, fine-tuning on classification tasks, and ECG feature extraction tasks.

3.1 Patch Masking

Let $x \in \mathbb{R}^{L \times T}$ represent a multi-lead ECG of length T with L channels. We divide the interval $[0, T]$ into N non-overlapping subintervals of length t . Each subinterval in each channel constitutes a patch of x , resulting in $L \times N$ patches. The masking strategy in multi-lead ECG must be carefully chosen because patches in different leads at the same temporal position are highly correlated, potentially making the prediction task too easy. To address this, we mask all patches across different leads in the same temporal space. With this in mind, we employ two masking strategies: *random masking* and *multi-block masking*.

In random masking, we randomly select a percentage of subintervals to mask, while in multi-block masking, we select multiple consecutive subintervals to mask. Note that we allow these consecutive subintervals to overlap, which requires the model to predict much longer sequences of representations. In this paper, we use both masking strategies to evaluate the effectiveness of ECG-JEPA, with a random masking ratio of (0.6, 0.7) and a multi-block masking ratio of (0.175, 0.225) with a frequency of 4. The unmasked patches serve as the contextual input for the student networks, while the masked patches are the ones for which we aim to predict the representations.

The patches are then converted into sequences of token vectors using a linear layer, and augmented with positional embeddings. For positional encoding, we employ the conventional 2-dimensional sinusoidal positional embeddings for the student and teacher networks, while we use 1-dimensional sinusoidal positional embeddings for the predictor network.

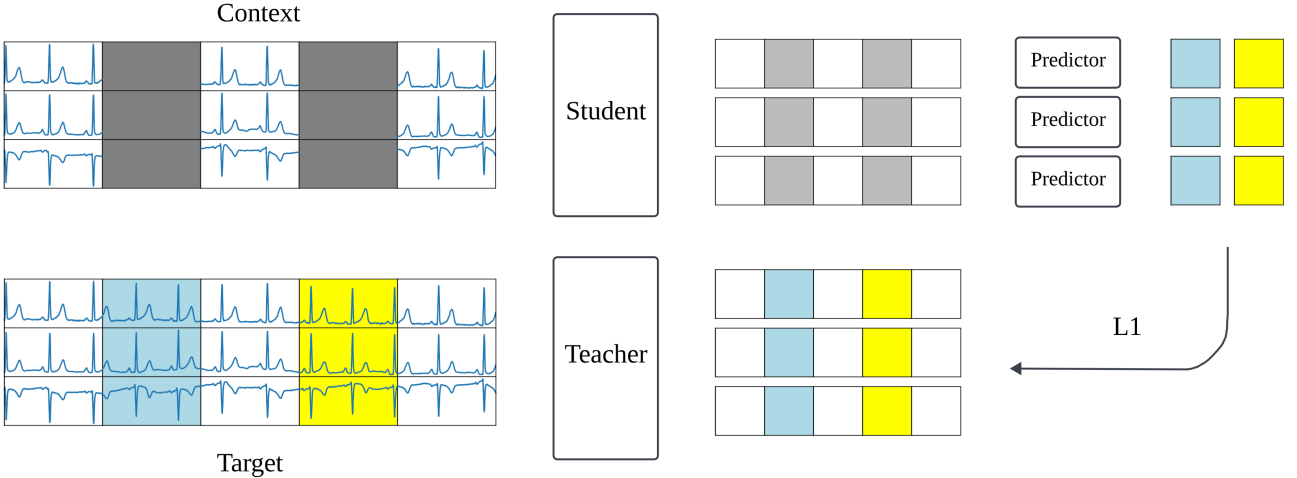


Figure 3: **ECG-JEPA**. The student network processes only non-masked patches of time series, whereas the teacher network processes the entire time series. Then the predictor predicts the representation of masked patches processed by the teacher. Note that both student and teacher network process the multi-channel time series, while predictor gets only a single-channel time series. In this picture, there are $L = 3$ leads with $N = 5$ subintervals and $Q = 3$ unmasked subintervals.

3.2 Teacher, Student, and Predictor

ECG-JEPA consists of three main components: the teacher network, the student network, and the predictor network. Both the teacher and student networks are based on standard transformer architectures. The weights of the teacher network are updated through an exponential moving average (EMA) of the student network, with details provided in the supplementary materials. The predictor network, a smaller transformer, operates on single-channel representations.

The teacher network handles the entire $L \times N$ patches, generating fully contextualized $L \times N$ representations. The student network, however, processes only $L \times Q$ visible (unmasked) patches, where $Q < N$ represents the number of visible time intervals. These $L \times Q$ representations from the student are then concatenated with the (learnable) mask tokens, resulting in $L \times N$ representations. Subsequently, each lead’s representations are passed to the predictor, which processes single-channel representations. The predictor’s output, the predicted representations of the target patches, is compared with the target representations using a smooth L1 loss function.

3.3 Cross-Pattern Attention (CroPA)

Biological signals often require simultaneous observation across multiple channels. In a 12-lead ECG, abnormalities must be consistent across multiple leads to diagnose specific cardiac pathologies. Therefore, the meaning of a single patch should be understood in the context of other patches within the same channel and across different channels. In contrast, patches in different channels and temporal spaces are often neglected when interpreting a 12-lead ECG.

To address this, we introduce *Cross-Pattern Attention (CroPA)*, a masked self-attention tailored for multi-lead ECG data. CroPA allows each patch to attend only to patches within the same channel and temporal space (Figure 4). This method enhances our model’s effectiveness compared to the standard attention mechanism, where patches attend to all other patches indiscriminately.

4 Related Work

This section provides an overview of existing SSL methods that have been applied to ECG data. We compare ECG-JEPA with these methods on various downstream tasks in the next section.

4.1 Contrastive Learning

Contrastive learning has been widely explored in various research works for its effectiveness in unsupervised representation learning. *Contrastive Predictive Coding (CPC)* [15] aims to capture useful data representations by predicting future

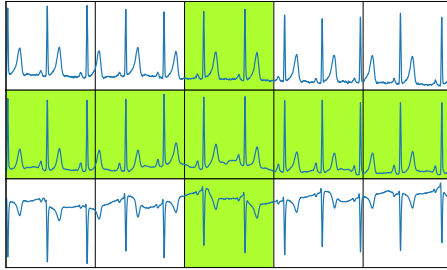


Figure 4: **Cross-Pattern Attention (CroPA)**. The patch in the middle attends only to the colored patches, which are in the same lead and temporal space.

observations in the latent space. It uses sequential data where the “true future” is treated as the positive sample, and other observations within the same sequence are treated as negative samples. *SimCLR* [7] and *MoCo* [16] also leverage contrastive approaches, with positive samples being augmented versions of the same image and negative samples being other images. *SimCLR* relies on large batch sizes and extensive data augmentation, while *MoCo* uses a momentum encoder to maintain a dynamic dictionary of encoded samples, enabling more stable training with smaller batch sizes.

4.2 Generative Architectures

BERT [4] pioneered generative architectures in natural language processing (NLP), inspiring similar methods in other domains. *Masked Autoencoders (MAE)* [8] have been developed for computer vision, where a portion of the input image is masked, and the model is trained to reconstruct these missing parts. Recently, [17] pointed out that generative architectures often prioritize learning the principal subspaces of the data, which may limit their effectiveness in capturing semantic representations for perceptual tasks.

4.3 Joint-Embedding Predictive Architectures

Data2vec [18] introduced an SSL architecture that predicts the average of the encoder’s final layers’ outputs, which was further improved in efficiency in *data2vec 2.0* [19]. Notable models like *I-JEPA* [9] and *V-JEPA* [11] predict the hidden representations of masked patches, enabling semantic representation learning for images and videos, respectively.

4.4 Self-Supervised Learning for ECG

Several attempts have been made to train SSL models for 12-lead ECG data. *Contrastive Multi-segment Coding (CMSC)* [20] is a contrastive method that divides an ECG into two segments, encouraging close representations for compatible segments while pushing apart incompatible ones. *Contrastive Predictive Coding (CPC)* [15] has also been used for ECG data in [21], predicting future representations of the ECG. A significant disadvantage of CPC is that it is not scalable to large datasets, as the LSTM modules inside CPC make the training process extremely slow. Recently, [22] utilized masked autoencoders for ECG data, proposing temporal and channel masking strategies, coined as *Masked Time Autoencoder (MTAE)* and *Masked Lead Autoencoder (MLAE)*, respectively. Similarly, [23] proposed *ST-MEM*, an MAE for ECG data that masks random time intervals for each lead. One possible drawback of MLAE and ST-MEM is that predicting some patches can be relatively easy considering that 12 leads signals are highly correlated.

5 Experimental Settings

This section provides an overview of the experimental settings. Details of all experiments can be found in the supplementary materials.

5.1 Pretraining Datasets

Training SSL models with large datasets is crucial for developing generalized representations. However, most previous works have used relatively small datasets, with the exception of [23], where an SSL model was trained with a large number of 12-lead ECGs. Following [23], we use the *Chapman* [24], *Ningbo* [25], and *CODE-15* [26] datasets for

pretraining ECG-JEPA. The Chapman and Ningbo datasets collectively consist of 45,152 10-second 12-lead ECGs at 500Hz. CODE-15 includes 345,779 12-lead ECGs from 233,770 patients at 400Hz, with 143,328 being 10-second recordings. After excluding recordings with missing values, we have 43,240 ECGs from Chapman and Ningbo and 130,900 ECGs from CODE-15. All ECGs were resampled to 250Hz for consistency.

5.2 Downstream Datasets

We use the *PTB-XL* [27] and *CPSC2018* [28] datasets to evaluate the performance of ECG-JEPA on downstream tasks. *PTB-XL* contains 21,837 clinical 10-second 12-lead ECG records from 18,885 patients, recorded at 500Hz and annotated with 71 diagnostic labels, which are aggregated into five superclasses. We use these superclass labels for our experiments. The *CPSC2018* dataset includes 6,877 12-lead ECG recordings with nine annotated cardiac conditions. These datasets are multi-label in nature, where each recording can have multiple labels simultaneously. The details of the datasets are provided in the supplementary materials.

5.3 Pretraining

After resampling the ECG data to 250Hz, each 10-second multi-lead ECG has $T = 2500$ time points. We divide the interval $[0, T]$ into $N = 50$ non-overlapping subintervals of length $t = 50$. The model is trained for 100 epochs without any data augmentations, and the final checkpoint is used for downstream tasks.

5.4 Architecture

We use vision transformer (ViT-Base) architectures [29] for the student and teacher network, and a smaller standard transformer architecture for the predictor network. The student and teacher network process the multi-lead ECG, while the predictor processes each lead independently to reconstruct the masked representations. See supplementary materials for detailed architecture specifications.

5.5 Downstream Tasks

We conduct extensive experiments to show that ECG-JEPA effectively captures semantic representations. We evaluate its performance on classification tasks through linear probing and fine-tuning. Additionally, we evaluate the performance on the low-shot setting, and on the reduced-lead setting where the downstream dataset is restricted to have a single or two leads.

Next, we validate the expressive power of the learned representations by predicting ECG features, including heart rate and QRS duration. To the best of our knowledge, this is the first work showing that the learned representations can recover various ECG features. The successful prediction of these features provides compelling evidence that the representations are not only informative but also capture essential and clinically relevant characteristics, making them highly reliable for ECG analysis.

In ECG analysis, it is common for a single recording to have multiple labels simultaneously, making datasets like *PTB-XL* and *CPSC2018* multi-label tasks. However, many previous studies have converted this into a multi-class classification problem by restricting the dataset to subsets with only a single label. To ensure a fair comparison, we will pretrain the methods using publicly available code and evaluate their performance on the multi-label classification task. If the code is not available, we will convert our task into a multi-class problem and compare the results with the reported performance in the literature.

6 Experiments

In this section, we assess the performance of the learned representations on various downstream tasks. Our experiments aim to demonstrate that the learned representations are generalizable and effective in capturing essential ECG features. We compare ECG-JEPA with several state-of-the-art SSL methods.

For classification tasks, we use AUC (Area Under the ROC Curve) and F1 scores as our primary evaluation metrics. AUC evaluates model performance across all possible thresholds, providing a comprehensive and stable measure of discriminative ability. In contrast, the F1 score balances precision and recall at a fixed threshold. In our experiments, we use the AUC as our main metric, as it provides a more robust evaluation of the model’s performance across varying classification thresholds, ensuring that the results are not overly dependent on a single decision boundary.

Table 1: **Linear evaluation on multi-label task.**

Method	Epochs	PTB-XL		CPSC2018	
		AUC	F1	AUC	F1
ST-MEM	800	0.896	0.662	0.964	0.752
SimCLR	300	0.866	0.624	0.890	0.523
CMSC	300	0.802	0.472	0.767	0.206
CPC	100	0.620	0.167	0.687	0.091
E-JEPA _{rb}	100	0.906	0.690	0.969	0.769
E-JEPA _{mb}	100	0.912	0.712	0.971	0.789

Table 2: **Linear evaluation on multi-class task.**

Method	Epochs	PTB-XL		CPSC2018	
		AUC	F1	AUC	F1
MoCo v3 ¹	800	0.739	0.142	0.712	0.080
MTAE ¹	800	0.807	0.437	0.818	0.349
MLAE ¹	800	0.779	0.382	0.794	0.263
ST-MEM	800	0.888	0.566	0.973	0.805
SimCLR	300	0.842	0.496	0.918	0.624
CMSC	300	0.796	0.442	0.787	0.391
CPC	100	0.600	0.201	0.672	0.210
E-JEPA _{rb}	100	0.894	0.616	0.974	0.805
E-JEPA _{mb}	100	0.896	0.628	0.973	0.819

For multi-label classification, the AUC is computed by averaging the scores of binary classifications for each label. For multi-class classification, the AUC is calculated using the average of one-vs-rest approach. In both cases, the F1 score is computed using a macro-averaged approach that averages the F1 scores of all classes.

In most cases, ECG-JEPA outperforms other SSL methods that leverage hand-crafted augmentations, demonstrating its effectiveness in learning general representations of ECG data. In experiments, E-JEPA_{rb} and E-JEPA_{mb} refer to ECG-JEPA models trained with random masking and multi-block masking strategies, respectively.

6.1 Linear Evaluation

Tables 1 and 2 present the results of our linear evaluation on the *PTB-XL* and *CPSC2018* datasets. We train a linear classifier on top of the frozen representations for 10 epochs, and evaluate its performance on downstream tasks. As shown in the tables, ECG-JEPA consistently outperforms other SSL methods, demonstrating superior efficiency and effectiveness with substantially reduced computational resources.

6.2 Fine-tuning

Fine-tuning is another method to evaluate the quality of learned representations, as it tests the model’s ability to adapt its pre-trained features to new tasks. In the fine-tuning process, we add a linear classification head at the end of the encoder and train the whole network for 10 epochs. Fine-tuning can potentially enhance performance beyond what is achieved with linear evaluation alone.

Table 3 presents the results of fine-tuning on the *PTB-XL* and *CPSC2018* datasets. ECG-JEPA is compared with other SSL methods in a multi-class classification setting. The results indicate that ECG-JEPA achieves the highest AUC and F1 scores on *PTB-XL* and the highest AUC on *CPSC2018*. These results highlight ECG-JEPA’s effectiveness in fine-tuning scenarios, demonstrating its ability to leverage transfer learning by refining and adapting its learned representations for improved performance in specific classification tasks.

¹Score as reported in [23].

²We did not fine-tune CPC due to its slow training process.

Table 3: Fine-tuning on multi-class task.

Method	Epochs	PTB-XL		CPSC2018	
		AUC	F1	AUC	F1
MoCo v3 ¹	800	0.913	0.644	0.967	0.838
MTAE ¹	800	0.910	0.613	0.961	0.769
MLAE ¹	800	0.915	0.625	0.973	0.816
CMSC ¹	800	0.877	0.510	0.938	0.717
ST-MEM	800	0.929	0.668	0.977	0.820
SimCLR	300	0.905	0.650	0.934	0.693
CPC ²	100	-	-	-	-
E-JEPA _{rb}	100	0.944	0.710	0.980	0.821
E-JEPA _{mb}	100	<u>0.937</u>	<u>0.680</u>	0.983	0.799

Table 4: Low-shot linear evaluation on the multi-label PTB-XL task. The mean and standard deviation of macro AUC are reported for 1% (192 samples) and 10% (1923 samples) of the training set, selected three times independently.

Method	Epochs	PTB-XL	
		1%	10%
ST-MEM	800	0.807 \pm 0.005	0.872 \pm 0.001
SimCLR	300	0.803 \pm 0.002	0.843 \pm 0.001
CMSC	300	0.750 \pm 0.008	0.792 \pm 0.001
CPC	100	0.523 \pm 0.006	0.560 \pm 0.005
E-JEPA _{rb}	100	<u>0.836 \pm 0.006</u>	<u>0.887 \pm 0.000</u>
E-JEPA _{mb}	100	0.843 \pm 0.004	0.894 \pm 0.003

6.3 Low-shot Linear Evaluation

Table 4 presents the performance comparison on the low-shot task. Low-shot learning is particularly challenging, as models must generalize effectively with limited labeled data. Given the difficulty and resource-intensive nature of obtaining labeled data in medical research, low-shot learning represents a realistic and critical scenario in the medical field. In this experiment, we evaluate the performance of ECG-SSL models on the *PTB-XL* multi-label task with only 1% and 10% of the training set, while keeping the test set fixed. As shown in the table, ECG-JEPA demonstrates a clear advantage over other SSL methods, with its effectiveness becoming particularly evident in low-shot learning tasks. This suggests that ECG-JEPA can be particularly well-suited for transfer learning where labeled data is scarce.

6.4 Reduced Lead Evaluation

Because transformer architectures can accept variable input lengths, we can evaluate ECG-JEPA’s performance on reduced lead tasks. In this experiment, we perform a linear evaluation on the *PTB-XL* multi-label task using reduced leads. Specifically, we utilize only a single lead (Lead II) and two leads (Lead II and V1), training linear classifiers on top of the learned representations for 10 epochs. We then compare ECG-JEPA’s performance with ST-MEM, another model supporting reduced lead evaluation. Table 5 presents the results of this reduced lead linear evaluation. Notably, ECG-JEPA performs well even in the reduced lead setting. This robustness is particularly valuable since most daily mobile devices typically output only one or two leads, highlighting ECG-JEPA’s potential for practical applications in mobile health monitoring.

Table 5: Reduced lead evaluation. Linear evaluation on PTB-XL multi-label task with reduced lead settings.

Method	1-Lead		2-Lead	
	AUC	F1	AUC	F1
ST-MEM	0.832	0.571	0.848	0.597
E-JEPA _{rb}	<u>0.846</u>	0.596	<u>0.877</u>	<u>0.647</u>
E-JEPA _{mb}	0.849	0.593	0.880	0.657

Table 6: **ECG feature extraction.** Means and standard deviations of absolute differences between the predicted and extracted values for heart rate and QRS duration. Small values indicate better performance. The final row provides the overall mean and standard deviation for both features across all samples in the PTB-XL test set.

Method	Heart Rate (BPM)	QRS Dur. (ms)
ST-MEM	1.35 ± 2.38	4.60 ± 4.16
SimCLR	1.87 ± 2.81	6.14 ± 5.80
CMSC	7.20 ± 7.43	10.12 ± 9.98
CPC	11.40 ± 11.04	11.55 ± 11.55
E-JEPA _{rb}	1.54 ± 2.62	4.81 ± 4.29
E-JEPA _{mb}	1.45 ± 2.44	4.41 ± 4.08
Mean	75.01 ± 17.65	90.48 ± 17.02

Table 7: **Effect of CroPA.** Linear evaluation (*lin*) and fine-tuning (*ft*) results on PTB-XL multi-class task with ECG-JEPA_{rb} and ECG-JEPA_{mb}. In both cases, CroPA improves the model’s performance.

Mask	CroPA	Epochs	<i>lin</i>	<i>ft</i>
			AUC	AUC
Random	x	100	0.888	0.930
	x	200	0.887	0.927
	o	100	0.894	0.944
Multi-block	x	100	0.872	0.924
	x	200	0.886	0.914
	o	100	0.896	0.937

6.5 ECG Feature Extraction

ECG features are essential for diagnosing and monitoring cardiac conditions. We evaluate the model’s ability to extract key ECG features, including heart rate and QRS duration, from the learned representations of the *PTB-XL* dataset. Unlike classification tasks, which are highly perceptual, ECG features are directly related to the morphology of the signal. For example, heart rate can be measured by the average distance between R-peaks, and QRS duration can be measured by the average width of the QRS complex.

Several methods have been proposed to segment ECG signals [30, 31, 32, 33]. Segmentation models can be used to extract ECG features. In this experiment, we employed a publicly available segmentation model [33] to extract ECG features from the PTB-XL dataset, which served as our ground truth labels. We then trained a linear regression model on the learned representations to predict these ECG features, using the mean squared error (MSE) as the loss function.

Table 6 presents the performance comparison, showing the means and standard deviations of the absolute differences between the extracted and predicted values across all samples in the PTB-XL test set.

Interestingly, although the model’s learned representations are implied to capture high-level features based on their strong performance in linear evaluation tasks across various datasets, they still retain the ability to recover low-level information, such as ECG features. This dual capability of capturing both high-level and low-level information is noteworthy and highlights the model’s versatility.

7 Ablation Study

7.1 Effect of CroPA

Table 7 presents the results of our evaluation of the effectiveness of CroPA. CroPA introduces a “human-like” inductive bias, enabling the model to be trained more efficiently on multi-lead ECG data. Without CroPA, models may require more epochs to converge. For a fair comparison, we trained ECG-JEPA with and without CroPA for 100 and 200 epochs and compared their performance on the PTB-XL multi-class task. The results show that CroPA considerably improves the model’s performance, demonstrating its effectiveness in capturing inter-lead relationships and enhancing the model’s ability to learn meaningful representations.

Table 8: **Effect of masking strategy.** Linear evaluation results on PTB-XL multi-label task using different masking ratios and strategies.

Mask	Ratio	Freq.	AUC	F1
Random	(0.3, 0.4)	1	0.884	0.652
Random	(0.4, 0.5)	1	0.904	0.698
Random	(0.5, 0.6)	1	0.906	0.697
Random	(0.6, 0.7)	1	0.906	0.690
Random	(0.7, 0.8)	1	0.909	0.706
Multi-block	(0.10, 0.15)	4	0.904	0.678
Multi-block	(0.15, 0.20)	4	0.905	0.687
Multi-block	(0.175, 0.225)	4	0.912	0.712

7.2 Masking Ratio

Table 8 presents the performance of ECG-JEPA in linear evaluation with different masking ratios and strategies. The results indicate that the model benefits from a high masking ratio. Notably, multi-block masking is advantageous for linear evaluation, while random masking is more effective for fine-tuning, as indicated in Table 3. Although random masking with a ratio of (0.7, 0.8) achieves better performance in the PTB-XL multi-label task, a masking ratio of (0.6, 0.7) performs better in other tasks. Therefore, we chose the latter for our main experiments.

8 Future Work

Our method has potential applications in various physiological multivariate signals, such as EEG and EMG. These signals share characteristics with ECG, including their multivariate nature and high dimensionality, making them suitable for our proposed approach.

Another promising direction involves the integration of multi-modal data. For example, multi-lead ECG data could be combined with other diagnostic modalities, such as chest X-rays (CXR), to provide a more comprehensive understanding of a patient’s condition.

One significant challenge in pursuing these extensions is the scarcity of large-scale datasets. Addressing this limitation is crucial for advancing and validating our method across diverse applications.

9 Conclusion

We proposed ECG-JEPA, a novel SSL method tailored for 12-lead ECG data. By utilizing a JEPA coupled with the innovative relative positional encoding method, CroPA, ECG-JEPA effectively learns meaningful representations of ECG signals. This approach addresses the challenges posed by noise and artifacts in ECG data, demonstrating substantial improvements over existing SSL methods in various downstream tasks, with the added benefit of significantly faster convergence.

Our extensive experimental evaluations reveal that ECG-JEPA outperforms state-of-the-art SSL methods across several tasks, including linear evaluation, fine-tuning, low-shot learning, and ECG feature extraction. Moreover, our investigation into the use of 8 leads, as opposed to the full 12-lead ECG, indicates that this reduction does not compromise performance while optimizing computational efficiency. This finding is particularly significant for applications constrained by limited computational resources.

References

- [1] Awni Y Hannun, Pranav Rajpurkar, Masoumeh Haghpanahi, Geoffrey H Tison, Codie Bourn, Mintu P Turakhia, and Andrew Y Ng. Cardiologist-level arrhythmia detection and classification in ambulatory electrocardiograms using a deep neural network. *Nature medicine*, 25(1):65–69, 2019.
- [2] Antônio H Ribeiro, Manoel Horta Ribeiro, Gabriela MM Paixão, Derick M Oliveira, Paulo R Gomes, Jéssica A Canazart, Milton PS Ferreira, Carl R Andersson, Peter W Macfarlane, Wagner Meira Jr, et al. Automatic diagnosis of the 12-lead ecg using a deep neural network. *Nature communications*, 11(1):1760, 2020.

- [3] Konstantinos C Siontis, Peter A Noseworthy, Zachi I Attia, and Paul A Friedman. Artificial intelligence-enhanced electrocardiography in cardiovascular disease management. *Nature Reviews Cardiology*, 18(7):465–478, 2021.
- [4] Jacob Devlin, Ming-Wei Chang, Kenton Lee, and Kristina Toutanova. Bert: Pre-training of deep bidirectional transformers for language understanding, 2019.
- [5] Tom Brown, Benjamin Mann, Nick Ryder, Melanie Subbiah, Jared D Kaplan, Prafulla Dhariwal, Arvind Neelakantan, Pranav Shyam, Girish Sastry, Amanda Askell, et al. Language models are few-shot learners. *Advances in neural information processing systems*, 33:1877–1901, 2020.
- [6] Hugo Touvron, Thibaut Lavigra, Gautier Izacard, Xavier Martinet, Marie-Anne Lachaux, Timothée Lacroix, Baptiste Rozière, Naman Goyal, Eric Hambro, Faisal Azhar, Aurelien Rodriguez, Armand Joulin, Edouard Grave, and Guillaume Lample. Llama: Open and efficient foundation language models, 2023.
- [7] Ting Chen, Simon Kornblith, Mohammad Norouzi, and Geoffrey Hinton. A simple framework for contrastive learning of visual representations. In *International conference on machine learning*, pages 1597–1607. PMLR, 2020.
- [8] Kaiming He, Xinlei Chen, Saining Xie, Yanghao Li, Piotr Dollár, and Ross Girshick. Masked autoencoders are scalable vision learners. In *Proceedings of the IEEE/CVF conference on computer vision and pattern recognition*, pages 16000–16009, 2022.
- [9] Mahmoud Assran, Quentin Duval, Ishan Misra, Piotr Bojanowski, Pascal Vincent, Michael Rabbat, Yann LeCun, and Nicolas Ballas. Self-supervised learning from images with a joint-embedding predictive architecture. In *Proceedings of the IEEE/CVF Conference on Computer Vision and Pattern Recognition*, pages 15619–15629, 2023.
- [10] Zhan Tong, Yibing Song, Jue Wang, and Limin Wang. Videomae: Masked autoencoders are data-efficient learners for self-supervised video pre-training. *Advances in neural information processing systems*, 35:10078–10093, 2022.
- [11] Adrien Bardes, Quentin Garrido, Jean Ponce, Xinlei Chen, Michael Rabbat, Yann LeCun, Mahmoud Assran, and Nicolas Ballas. Revisiting feature prediction for learning visual representations from video, 2024.
- [12] Hong Liu, Jeff Z. HaoChen, Adrien Gaidon, and Tengyu Ma. Self-supervised learning is more robust to dataset imbalance, 2022.
- [13] Pascal Vincent, Hugo Larochelle, Yoshua Bengio, and Pierre-Antoine Manzagol. Extracting and composing robust features with denoising autoencoders. In *Proceedings of the 25th international conference on Machine learning*, pages 1096–1103, 2008.
- [14] Yann LeCun. A path towards autonomous machine intelligence version 0.9. 2, 2022-06-27. <https://openreview.net/forum?id=BZ5a1r-kVsf>, 2022. Accessed: 2024-06-01.
- [15] Aaron van den Oord, Yazhe Li, and Oriol Vinyals. Representation learning with contrastive predictive coding, 2019.
- [16] Kaiming He, Haoqi Fan, Yuxin Wu, Saining Xie, and Ross Girshick. Momentum contrast for unsupervised visual representation learning. In *Proceedings of the IEEE/CVF conference on computer vision and pattern recognition*, pages 9729–9738, 2020.
- [17] Randall Balestriero and Yann LeCun. Learning by reconstruction produces uninformative features for perception, 2024.
- [18] Alexei Baevski, Wei-Ning Hsu, Qiantong Xu, Arun Babu, Jiatao Gu, and Michael Auli. Data2vec: A general framework for self-supervised learning in speech, vision and language. In *International Conference on Machine Learning*, pages 1298–1312. PMLR, 2022.
- [19] Alexei Baevski, Arun Babu, Wei-Ning Hsu, and Michael Auli. Efficient self-supervised learning with contextualized target representations for vision, speech and language. In *International Conference on Machine Learning*, pages 1416–1429. PMLR, 2023.
- [20] Dani Kiyasseh, Tingting Zhu, and David A Clifton. Clocs: Contrastive learning of cardiac signals across space, time, and patients. In *International Conference on Machine Learning*, pages 5606–5615. PMLR, 2021.
- [21] Temesgen Mehari and Nils Strodthoff. Self-supervised representation learning from 12-lead ecg data. *Computers in biology and medicine*, 141:105114, 2022.
- [22] Huaicheng Zhang, Wenhan Liu, Jiguang Shi, Sheng Chang, Hao Wang, Jin He, and Qijun Huang. Maefe: Masked autoencoders family of electrocardiogram for self-supervised pretraining and transfer learning. *IEEE Transactions on Instrumentation and Measurement*, 72:1–15, 2022.

- [23] Yeongyeon Na, Minje Park, Yunwon Tae, and Sungsoon Joo. Guiding masked representation learning to capture spatio-temporal relationship of electrocardiogram, 2024.
- [24] Jianwei Zheng, Jianming Zhang, Sidy Danioko, Hai Yao, Hangyuan Guo, and Cyril Rakovski. A 12-lead electrocardiogram database for arrhythmia research covering more than 10,000 patients. *Scientific data*, 7(1):48, 2020.
- [25] Jianwei Zheng, Huimin Chu, Daniele Struppa, Jianming Zhang, Sir Magdi Yacoub, Hesham El-Askary, Anthony Chang, Louis Ehwerhemuepha, Islam Abudayyeh, Alexander Barrett, et al. Optimal multi-stage arrhythmia classification approach. *Scientific reports*, 10(1):2898, 2020.
- [26] Yu-Jhen Chen, Chien-Liang Liu, Vincent S Tseng, Yu-Feng Hu, and Shih-Ann Chen. Large-scale classification of 12-lead ecg with deep learning. In *2019 IEEE EMBS international conference on biomedical & health informatics (BHI)*, pages 1–4. IEEE, 2019.
- [27] Patrick Wagner, Nils Strothoff, Ralf-Dieter Bousseljot, Dieter Kreiseler, Fatima I Lunze, Wojciech Samek, and Tobias Schaeffter. PtB-XL, a large publicly available electrocardiography dataset. *Scientific data*, 7(1):1–15, 2020.
- [28] Feifei Liu, Chengyu Liu, Lina Zhao, Xiangyu Zhang, Xiaoling Wu, Xiaoyan Xu, Yulin Liu, Caiyun Ma, Shoushui Wei, Zhiqiang He, et al. An open access database for evaluating the algorithms of electrocardiogram rhythm and morphology abnormality detection. *Journal of Medical Imaging and Health Informatics*, 8(7):1368–1373, 2018.
- [29] Alexey Dosovitskiy, Lucas Beyer, Alexander Kolesnikov, Dirk Weissenborn, Xiaohua Zhai, Thomas Unterthiner, Mostafa Dehghani, Matthias Minderer, Georg Heigold, Sylvain Gelly, Jakob Uszkoreit, and Neil Houlsby. An image is worth 16x16 words: Transformers for image recognition at scale, 2021.
- [30] Iana Sereda, Sergey Alekseev, Aleksandra Koneva, Roman Kataev, and Grigory Osipov. Ecg segmentation by neural networks: Errors and correction. In *2019 International Joint Conference on Neural Networks (IJCNN)*, pages 1–7. IEEE, 2019.
- [31] Viktor Moskalenko, Nikolai Zolotykh, and Grigory Osipov. Deep learning for ecg segmentation. In *Advances in Neural Computation, Machine Learning, and Cognitive Research III: Selected Papers from the XXI International Conference on Neuroinformatics, October 7–11, 2019, Dolgoprudny, Moscow Region, Russia*, pages 246–254. Springer, 2020.
- [32] Zhenqin Chen, Mengying Wang, Meiyu Zhang, Wei Huang, Hanjie Gu, and Jinshan Xu. Post-processing refined ecg delineation based on 1d-unet. *Biomedical Signal Processing and Control*, 79:104106, 2023.
- [33] Chankyu Joung, Mijin Kim, Taejin Paik, Seong-Ho Kong, Seung-Young Oh, Won Kyeong Jeon, Jae-hu Jeon, Joong-Sik Hong, Wan-Joong Kim, Woong Kook, et al. Deep learning based ecg segmentation for delineation of diverse arrhythmias. *PloS one*, 19(6):e0303178, 2024.
- [34] Priya Goyal, Piotr Dollár, Ross Girshick, Pieter Noordhuis, Lukasz Wesolowski, Aapo Kyrola, Andrew Tulloch, Yangqing Jia, and Kaiming He. Accurate, large minibatch sgd: Training imagenet in 1 hour, 2018.
- [35] Kaiming He, Xiangyu Zhang, Shaoqing Ren, and Jian Sun. Deep residual learning for image recognition. In *Proceedings of the IEEE conference on computer vision and pattern recognition*, pages 770–778, 2016.

A Supplementary Materials

A.1 Experimental Details on ECG-JEPA

Hyperparameters for ECG-JEPA pretraining, linear evaluation, and fine-tuning are provided in Tables 9, 10, and 11, respectively. In ECG-JEPA_{mb}, the number of visible patches in ECG-JEPA_{mb} varies more than in ECG-JEPA_{rb}, resulting in higher GPU memory usage. Consequently, we reduced the batch size to 64 to fit the model on a single NVIDIA RTX 3090 GPU. Interestingly, ECG-JEPA_{mb} benefits from larger learning rates, even with the halved batch size.

For fine-tuning process, the actual learning rate is calculated as $lr = base_lr \times batchsize/256$, following the heuristic by [34].

Table 9: Pretraining Settings for ECG-JEPA.

config	ECG-JEPA _{rb}	ECG-JEPA _{mb}
optimizer	AdamW	AdamW
learning rate	2.5e-5	5e-5
weight decay	0.05	0.05
batch size	128	64
learning rate schedule	cosine decay	cosine decay
warmup epochs	5	5
epochs	100	100
drop path	0.1	0.1

Table 10: Linear Evaluation Settings

config	value
optimizer	AdamW
learning rate	5e-4
weight decay	0.05
batch size	32
learning rate schedule	cosine decay
warmup epochs	3
epochs	10

Table 11: Fine-tuning Settings.

config	value
optimizer	AdamW
base learning rate	1.0e-4
weight decay	0.05
batch size	16
learning rate schedule	cosine decay
warmup epochs	3
epochs	10

A.2 Pretraining Other SSL Models

Besides pretraining ECG-JEPA, we also pretrained other models, including CMSC [20], CPC [15], and SimCLR [7] using the same datasets as ECG-JEPA.

For CMSC and CPC, we adhered to the original architecture and hyperparameters. SimCLR utilized a ResNet50 [35] encoder with an output dimension of 2048. CMSC and SimCLR were pretrained for 300 epochs, selecting the best checkpoint at 100, 200, or 300 epochs based on linear evaluation performance on the PTB-XL multi-label setting. Due to the slow training process, CPC was pretrained for only 100 epochs, taking approximately 9 days on a single NVIDIA

RTX 3090 GPU due to the LSTM module in the model. For ST-MEM [23], we employed the publicly available checkpoint pretrained for 800 epochs.

Given SimCLR’s sensitivity to data augmentations, we applied several that work well empirically: baseline shift (adding a constant to all leads), baseline wander (low-frequency noise), Gaussian noise (random noise), powerline noise (50Hz noise), channel resize, random crop, and jump noise (sudden jumps). These augmentations aimed to enhance the robustness of the model to various signal distortions.

A.3 Downstream Datasets Details

Table 12, 13, 14, and 15 show the distribution of the PTB-XL and CPSC2018 datasets in both multi-label and multi-class settings.

The PTB-XL dataset is stratified into ten folds, where the first eight folds are used for training, the ninth fold for validation, and the tenth fold for testing. In our experiments, we used the first nine folds for training and the tenth fold for testing, as we did not observe overfitting during linear evaluation and fine-tuning.

For the CPSC2018 dataset, only the training set is publicly available, which is stratified into seven folds. We used the first six folds for training and the seventh fold for testing, omitting the validation set. The original CPSC2018 dataset consists of 6,877 ECG recordings, but we excluded recordings with a length of less than 10 seconds, resulting in 6,867 ECG recordings.

Table 12: **PTB-XL multi-label distribution.** The sum of samples in each class exceeds the total number of ECG recordings due to the multi-label nature of the dataset.

	# ECG	Norm	MI	STTC	CD	HYP
Multi-label	21799	9514	5469	5235	4898	2649
Train	19230	8551	4919	4714	4402	2387
Test	2158	963	550	521	496	262

Table 13: **PTB-XL multi-class distribution.** ECGs with multiple labels are excluded from the PTB-XL multi-label dataset.

	# ECG	Norm	MI	STTC	CD	HYP
Multi-class	16244	9069	2532	2400	1708	535
Train	14594	8157	2276	2158	1524	479
Test	1650	912	256	242	184	56

Table 14: **CPSC2018 multi-label distribution.** The sum of samples in each class exceeds the total number of ECG recordings due to the multi-label nature of the dataset.

	# ECG	Norm	PVC	AF	LBBB	STE	1AVB	PAC	STD	RBBB
Multi-label	6867	918	1220	235	220	721	614	699	868	1854
Train	5989	805	1059	206	197	632	534	615	742	1616
Test	878	113	161	29	23	89	80	84	126	238

Table 15: **CPSC2018 multi-class distribution.** The number of ECG recordings for each superclass in the PTB-XL dataset. Note that the sum of samples in each class exceeds the total number of ECG recordings due to multi-label the nature of the dataset.

	# ECG	Norm	PVC	AF	LBBB	STE	1AVB	PAC	STD	RBBB
Multi-class	6391	918	975	178	185	685	531	606	783	1530
Train	5577	805	849	159	169	600	459	534	671	1331
Test	814	113	126	19	16	85	72	72	112	199

A.4 Exponential Moving Average

The teacher network is initialized as a copy of the student network and is updated using an exponential moving average (EMA) of the student's weights. The EMA is computed as follows:

$$\theta_{\text{teacher}}^i = \beta_i \theta_{\text{teacher}}^{i-1} + (1 - \beta_i) \theta_{\text{student}}^i$$

where i denotes the current training iteration, and β_i is a momentum parameter that evolves during training. The momentum parameter β_i is computed as:

$$\beta_i = \text{ema}_0 + \frac{i \cdot (\text{ema}_1 - \text{ema}_0)}{\text{iterations_per_epoch} \cdot \text{epochs}}$$

Here, ema_0 and ema_1 represent the initial and final values of the momentum parameter, respectively. For our implementation, $\text{ema}_0 = 0.996$ and $\text{ema}_1 = 1.0$.

A.5 Sufficiency of 8 Leads in ECG Analysis

In a standard 12-lead ECG, leads III, aVR, aVL, and aVF can be derived from leads I and II, as shown by the following equations:

$$\begin{aligned} \text{III} &= \text{II} - \text{I} \\ \text{aVR} &= -\frac{(\text{I} + \text{II})}{2} \\ \text{aVL} &= \text{I} - \frac{\text{II}}{2} \\ \text{aVF} &= \text{II} - \frac{\text{I}}{2} \end{aligned}$$

These derivations demonstrate that leads III, aVR, aVL, and aVF do not provide additional independent information beyond what is captured by leads I and II. Therefore, using only 8 leads (I, II, V1, V2, V3, V4, V5, and V6) can be sufficient for effective ECG analysis. This simplification not only reduces the computational load but also maintains the diagnostic integrity of the analysis.

A.6 Comparison with 12-Lead Model

We now investigate the practical sufficiency of using 8 leads for ECG-JEPA pretraining. To evaluate the impact of this reduction, we trained models using both 8 leads and 12 leads and compared their performance on the linear evaluation of a multi-label task for PTB-XL.

Table 16 presents the results of this comparison using ECG-JEPA_{rb}. As expected, the performance difference between the 8-lead and 12-lead models is minimal, indicating that using 8 leads is sufficient for effective pretraining without significant loss of information.

Table 16: **Comparison of 8-Lead and 12-Lead Models.**

Model	epochs	AUC	F1
8-Lead	100	0.906	0.690
12-Lead	100	0.905	0.699